

# Optimizing Graph Structure for Targeted Diffusion

Sixie Yu<sup>\*1</sup>, Leonardo Torres<sup>2</sup>, Scott Alfeld<sup>3</sup>, Tina Eliassi-Rad<sup>2</sup>, and Yevgeniy Vorobeychik<sup>1</sup>

<sup>1</sup>Washington University in St. Louis

<sup>2</sup>Northeastern University

<sup>3</sup>Amherst College

## Abstract

The problem of diffusion control on networks has been extensively studied, with applications ranging from marketing to cybersecurity. However, in many applications, such as targeted vulnerability assessment or clinical therapies, one aspires to affect a *targeted* subset of a network, while limiting the impact on the rest. We present a novel model in which the principal aim is to optimize graph structure to affect such targeted diffusion. We present an algorithmic approach for solving this problem at scale, using a gradient-based approach that leverages Rayleigh quotients and pseudospectrum theory. In addition, we present a condition for certifying a targeted subgraph as immune to targeted diffusion. Finally, we demonstrate the effectiveness of our approach through experiments on real and synthetic networks.

## 1 Introduction

Many diverse phenomena that propagate through a network, such as epidemic spread, cascading failures, and networks of chemical reactions, can be modeled by network diffusion models [3, 5, 23, 41, 38]. The problem of controlling diffusion has, as a result, received prominent attention in the literature, with primary focus on two mechanisms for control: the choice of initial nodes to start the spread [14, 7, 43], and the modification of network structure [16, 32, 42, 33]. To date, most work on diffusion control (either promotion or inhibition) has considered diffusion over the entire network. However, in many problems, the focus is instead on diffusion that is *targeted* to a particular subset of the network. For example, in cybersecurity, diffusion commonly models malware spread, but malware attacks are often targeted at particular subsets of critical devices [12], which should be accounted for in vulnerability analysis. Congestion cascades of ground traffic or flight networks are other examples, where the goal of resilience may be to ensure that cascades, should they occur, concentrate on a subset of high-capacity nodes that can handle them, limiting the impact on the rest of the network [10, 9]. Finally, medical treatments for certain diseases such as cancer may leverage a molecular signaling network, with the goal of targeting just the pathogenic portion of it, while limiting the deleterious effects on the rest [39].

We study the problem of targeted diffusion in which a principal<sup>1</sup> can modify the graph structure  $G = (\mathcal{V}, \mathcal{E})$  to achieve two goals: 1) maximize the diffusion spread to a target subgraph  $G_{\mathcal{S}}$ , and 2) minimize the impact on the remaining graph  $G \setminus G_{\mathcal{S}}$ . We capture the first goal by maximizing a utility function that incorporates spectral information of the adjacency matrix of  $G$ , specifically its largest (in module) eigenvalue, eigenvector centrality, and the normalized cut of the target subgraph. The second goal is achieved by limiting the modifications made outside of the target subgraph. We present a scalable algorithmic framework for solving this

---

<sup>\*</sup>sixie.yu@wustl.edu

<sup>1</sup>The principal is the agent who initiates diffusion.

problem. Our framework leverages a combination of gradient ascent with the use of Rayleigh quotients and pseudospectrum theory, which yields differentiable approximations of our objective and allows us to avoid projection steps that would otherwise be costly and imprecise. Moreover, we derive a condition that enables us to certify if a network is robust against a broad class of targeted diffusions. Finally, we demonstrate the effectiveness of our approach through extensive experiments.

**Related Work:** Various dynamical processes can be modeled as diffusion dynamics on networks, including the spread of infectious diseases [3, 5], cascading failures in infrastructure networks [23, 41], and information spread (e.g., rumors, fake news) on social networks [19, 20]. One line of research assesses the impact of cascading failures. Yang et al. [41] simulated cascading failures to quantify the vulnerability of the power grid in North America. Fleurquin et al. [10] studied the impact of flight delays as a cascading failure diffusing through the network. Motter and Lai [23] investigated the cascading failures on a network due to the malfunction of a single node. Another line of research concerns diffusion control, for example, selecting a set of nodes such that if the diffusion originated from them, it reaches as many nodes as possible [14, 7, 43]; or modifying network structures to increase or limit some diffusion [32, 28]. However, these lines of research do not differentiate between targeted and non-targeted nodes. Ho et al. [13] studied targeted diffusion controlled by changing nodal status. We focus on optimizing underlying network structures.

Another relevant research thread is network design, which is the problem of modifying network structure to induce certain desirable outcomes. Some prior work [32, 42, 31] considered the containment of spreading dynamics by adding or removing nodes or edges from the network, while others [37, 29, 16, 6, 22, 33] considered limiting the spread of infectious disease by minimizing the largest eigenvalue of the network. Kempe et al. [15] studied modifying network structure to induce certain outcomes from a game-theoretic perspective, but they did not consider diffusion dynamics. Others have studied the problem of manipulating node centrality measures (e.g., eigenvector or PageRank centrality) [2, 1] or node similarity measures (e.g., Katz similarity) [44] through edge perturbation. All of these prior efforts focus on the impact either at the network level or at the node-level properties, while our focus is on the impact of diffusion dynamics on a targeted subgraph of the network.

## 2 Model

We present a model for targeted diffusion through graph structure optimization. We refer to the agent who initiates diffusion as *the principal*. We use cybersecurity as a running example, where the principal (in this case, an attacker or an IT professional performing vulnerability assessment) initiates the diffusion (e.g., the spread of malware) on a network of computers. We define the impact of the diffusion as the number of infected (e.g., compromised with malware) nodes. The principal has two objectives: 1) she wishes to maximize the impact of the diffusion on a targeted set of nodes (e.g., computing nodes with access to critical assets), and 2) to limit the impact on non-targeted nodes to ensure stealth [12].

Let  $G = (\mathcal{V}, \mathcal{E})$  be a connected, undirected, possibly weighted, graph with no self-loops. Let  $n = |\mathcal{V}|$  be the number of nodes in  $G$  and  $\mathbf{A}$  be its adjacency matrix. Throughout this paper, the eigenvalues of  $\mathbf{A}$  are ranked in descending order  $\lambda_1(\mathbf{A}) \geq \dots \geq \lambda_n(\mathbf{A})$ . Suppose the principal targets a subgraph  $G_{\mathcal{S}}$  where  $\mathcal{S} \subseteq \mathcal{V}$  is the node set of  $G_{\mathcal{S}}$ . Let  $\mathcal{S}' = \mathcal{V} \setminus \mathcal{S}$ , and its induced subgraph  $G_{\mathcal{S}'}$ . Throughout the paper we assume  $G_{\mathcal{S}}$  is connected, and denote its adjacency matrix by  $\mathbf{A}_{\mathcal{S}}$ . To achieve her objectives, the principal modifies the structure of  $G$ . The modified

graph and targeted subgraph are represented by  $\tilde{G}$  and  $\tilde{G}_{\mathcal{S}}$ , respectively. Formally, the principal’s action is to add a perturbation  $\mathbf{\Delta} \in \mathbb{R}^{n \times n}$  to  $\mathbf{A}$ , which results in the perturbed adjacency matrix  $\tilde{\mathbf{A}} = \mathbf{A} + \mathbf{\Delta}$ . The adjacency matrix of  $\tilde{G}_{\mathcal{S}}$  is denoted by  $\tilde{\mathbf{A}}_{\mathcal{S}}$ .

## 2.1 Diffusion Dynamics

The status of a node is modeled by the well-known SIS (Susceptible-Infected-Susceptible) diffusion dynamics, where it alternates between “infected” and “susceptible”.<sup>2</sup> Due to the malware spread by infected neighbors, a susceptible node becomes infected with probability  $\beta$ . An infected node becomes susceptible again (e.g., malware is removed) with probability  $\delta$ . Following [5], this process is modeled by a nonlinear dynamical system. Let  $\pi_i$  be the probability of node  $i$  becoming infected (e.g., compromised with malware) in the steady state of this dynamical system, with  $\boldsymbol{\pi}$  the vector of these probabilities. A key result in [5] is that when  $\lambda_1(\mathbf{A}) < \delta/\beta$  the system converges to the steady state  $\boldsymbol{\pi} = \mathbf{0}$ , which implies that the diffusion process quickly dies out. However, when  $\lambda_1(\mathbf{A}) \geq \delta/\beta$  the system converges to another steady state  $\boldsymbol{\pi} \neq \mathbf{0}$ . We leverage this connection between graph structure, dynamical model of epidemic spread, and the epidemic threshold, in constructing our *threat model*, as discussed next.

## 2.2 Threat Model

**Maximizing the Impact on  $G_{\mathcal{S}}$ :** To maximize the impact of diffusion on  $G_{\mathcal{S}}$ , the principal has two goals: 1) ensure that epidemics starting in  $G_{\mathcal{S}}$  spread rather than die out, and 2) ensure that epidemics starting outside  $G_{\mathcal{S}}$  are likely to reach it. We capture the first goal by maximizing the largest (in module) eigenvalue of  $G_{\mathcal{S}}$ ,  $\lambda_1(\tilde{\mathbf{A}}_{\mathcal{S}})$ , which corresponds to the epidemic threshold of the targeted subgraph. The second goal is captured by maximizing the *normalized cut* of  $G_{\mathcal{S}}$ ,  $\phi(\mathcal{S})$ , where  $\mathcal{S}$  is the set of nodes in  $G_{\mathcal{S}}$  and  $\mathcal{S}'$  are the nodes in the remaining graph. The normalized cut is formally defined as follows:

$$\phi(\mathcal{S}) = \text{cut}(\mathcal{S}, \mathcal{S}') \left( \frac{1}{\text{vol}(\mathcal{S})} + \frac{1}{\text{vol}(\mathcal{S}')} \right), \quad (1)$$

where  $\text{cut}(\mathcal{S}, \mathcal{S}')$  is the sum of the weights on the edges across  $\mathcal{S}$  and  $\mathcal{S}'$  (unit weights for unweighted graphs), and  $\text{vol}(\mathcal{S})$  (resp.  $\text{vol}(\mathcal{S}')$ ) is the sum of degrees of the nodes in  $\mathcal{S}$  (resp.  $\mathcal{S}'$ ). The formal rationale for using the normalized cut is based on Meila et al. [21], which showed that increasing  $\phi(\mathcal{S})$  increases the probability that a random walker transitions from  $\mathcal{S}'$  to  $\mathcal{S}$ , if we assume that  $G_{\mathcal{S}}$  is smaller than  $G_{\mathcal{S}'}$ .

**Limiting the Impact on  $G_{\mathcal{S}'}$ :** Another important objective of the principal is to limit the impact on  $G_{\mathcal{S}'}$ , the non-targeted part of the graph. The first way we capture this goal is by limiting the likelihood of the epidemic spreading to  $G_{\mathcal{S}'}$ , which we define as minimizing the impact  $I(G_{\mathcal{S}'}) = \sum_{i \in \mathcal{S}'} \pi_i$ . We now demonstrate that minimizing  $I(G_{\mathcal{S}'})$  is approximately equivalent to minimizing the eigenvector centrality of  $\mathcal{S}'$ .

Let  $\mathbf{P}^t$  be the global configuration of the graph at time step  $t$ , where  $P_i^t$  is the probability that node  $i$  is infected (e.g., compromised with malware). According to [36] (see Section IV), for an arbitrary node  $i$ , ignoring higher-order terms involving  $P_i^t$  and taking the time step to be

---

<sup>2</sup>Our targeted diffusion model generalizes to other common diffusion dynamics such as SIR (Susceptible-Infected-Recovered) and SEIR (Susceptible-Exposed-Infected-Recovered). See Appendix 1 for a discussion.

infinitesimally small, the dynamics of  $P_i^t$  is modeled as the following:

$$\frac{dP_i^t}{dt} = \sum_{j \in \mathcal{V}} \beta \tilde{A}_{ij} P_j^t - \delta P_i^t. \quad (2)$$

Here, we can think of the two terms on the right side as two competing forces. The first term is the force contributed by the infected neighbors of node  $i$  (which increases  $P_i^t$ ), while the second term is the force due to  $i$ 's self recovery (which decreases  $P_i^t$ ). Rewriting in matrix notation yields:

$$\frac{d\mathbf{P}^t}{dt} = [\beta \tilde{\mathbf{A}} - \delta \mathbf{I}] \mathbf{P}^t, \quad (3)$$

which gives a linear approximation to the non-linear dynamical system proposed in [5]. The steady state  $\boldsymbol{\pi}$  must satisfy  $[\beta \tilde{\mathbf{A}} - \delta \mathbf{I}] \boldsymbol{\pi} = \mathbf{0}$ , which is equivalent to  $\tilde{\mathbf{A}} \boldsymbol{\pi} = (\delta/\beta) \boldsymbol{\pi}$ . Suppose  $\lambda_1(\tilde{\mathbf{A}}) = \delta/\beta$ , and  $\boldsymbol{\pi}$  is the corresponding eigenvector. Let  $\tilde{\mathbf{v}}_1$  be the unit eigenvector associated with  $\lambda_1(\tilde{\mathbf{A}})$ . Let  $\sigma(\mathcal{S}) = \sum_{j \in \mathcal{S}} \tilde{v}_1[j]$  be the eigenvector centrality of  $\mathcal{S}$ . Noting that  $\boldsymbol{\pi}$  may differ from  $\tilde{\mathbf{v}}_1$  by up to a multiplicative constant  $c$ , the impact on  $G_{\mathcal{S}'}$  can be approximated as:

$$I(G_{\mathcal{S}'}) = \sum_{j \in \mathcal{S}'} \pi_j \approx c \sum_{j \in \mathcal{S}'} \tilde{v}_1[j] = c(1 - \sigma(\mathcal{S})), \quad (4)$$

where the last equality is because  $\mathcal{S}$  and  $\mathcal{S}'$  are disjoint and  $\tilde{\mathbf{v}}_1$  is a unit vector. Thus, minimizing the impact on  $G_{\mathcal{S}'}$  is approximately equivalent to maximizing the eigenvector centrality of  $\mathcal{S}$ .

Recall that to have an epidemic spread, one needs  $\lambda_1(\tilde{\mathbf{A}}) \geq \delta/\beta$ . Here, we assumed  $\lambda_1(\tilde{\mathbf{A}}) = \delta/\beta$ . In Section 5, we demonstrate that our analysis yields an approach that is effective even when this assumption fails to hold (i.e., when  $\lambda_1(\tilde{\mathbf{A}}) > \delta/\beta$ ).

The second way in which we limit the impact on the underlying graph is by limiting the impact of the principal on the spectrum of  $\mathbf{A}$ .<sup>3</sup> Formally, this notion is captured through the following constraints:

$$|\lambda_i(\tilde{\mathbf{A}}) - \lambda_i(\mathbf{A})| \leq \epsilon, \quad i = 1, \dots, n, \quad (5)$$

where  $\epsilon > 0$  can be thought as the principal's budget.

In summary, the principal aims to (i) maximize the impact on  $G_{\mathcal{S}}$  through maximizing  $\lambda_1(\tilde{\mathbf{A}}_{\mathcal{S}})$  while (ii) limiting the impact on  $G_{\mathcal{S}'}$  by maximizing the eigenvector centrality  $\sigma(\mathcal{S})$ , and satisfying Eq. (5). Formally, the principal aims to solve the following optimization problem:

$$\begin{aligned} \max_{\tilde{\mathbf{A}}} \quad & \alpha_1 \lambda_1(\tilde{\mathbf{A}}_{\mathcal{S}}) + \alpha_2 \sigma(\mathcal{S}) + \alpha_3 \phi(\mathcal{S}) \\ \text{s.t.} \quad & \tilde{\mathbf{A}} \in \mathcal{P} = \left\{ \tilde{\mathbf{A}} \left| \begin{array}{l} |\lambda_i(\tilde{\mathbf{A}}) - \lambda_i(\mathbf{A})| \leq \epsilon, \quad i = 1, \dots, n, \\ \tilde{\mathbf{A}} = \tilde{\mathbf{A}}^\top, \tilde{\mathbf{A}}_{ii} = 0, \quad \forall i = 1, \dots, n \end{array} \right. \right\}, \end{aligned} \quad (6)$$

where the relative importance of the terms is balanced by the nonnegative constants  $\alpha_1, \alpha_2, \alpha_3$ , and the restrictions  $\tilde{\mathbf{A}} = \tilde{\mathbf{A}}^\top$  and  $\tilde{\mathbf{A}}_{ii} = 0, \forall i = 1, \dots, n$  ensure that  $\tilde{\mathbf{A}}$  is a valid adjacency matrix.

<sup>3</sup>In cybersecurity, there are natural interpretations of an attack's stealth. See Appendix 2 for further details.

### 3 Algorithm

To solve the optimization problem in Eq. (6), a natural approach would be to use a form of projected gradient ascent. There are, however, two major hurdles to this basic approach: 1) the objective function involves terms that do not have an explicit functional representation in the decision variables, and 2) the projection step is quite expensive, as it involves projecting into a spectral norm ball, which entails an expensive SVD operation [17]. We address these challenges in Algorithm 1, which is our gradient-based solution to the principal’s optimization problem as described in Eq. (6).

---

#### Algorithm 1 Gradient Ascent Algorithm

---

```

1: Input:  $\mathbf{A}, \epsilon, \{\eta_i\}_{i=1}$  ▷  $\{\eta_i\}_{i=1}$  is a schedule of step sizes
2: Initialize:  $i = 1, \mathbf{A}_1 = \mathbf{A}, B_1 = 0$  ▷  $B_i$ : the amount of budget used just before step  $i$ 
3: while True do
4:   Set  $\mathbf{\Delta}_i$  to the gradient of  $\alpha_1 \lambda_1(\tilde{\mathbf{A}}_{\mathcal{S}}) + \alpha_2 \sigma(\mathcal{S}) + \alpha_3 \phi(\mathcal{S})$  w.r.t. to  $\tilde{\mathbf{A}}_i$ 
5:   Set the diagonal entries of  $\mathbf{\Delta}_i$  to zeros
6:   if  $\|\mathbf{\Delta}_i\| = \mathbf{0}$  then ▷ a local optimum is found
7:     return  $\tilde{\mathbf{A}}_i$ 
8:   end if
9:   if  $B_i + \|\eta_i \mathbf{\Delta}_i\|_2 \leq \epsilon$  then ▷ one-step look ahead
10:     $\mathbf{A}_{i+1} = \mathbf{A}_i + \eta_i \mathbf{\Delta}_i, B_{i+1} = B_i + \|\eta_i \mathbf{\Delta}_i\|_2, i = i + 1$ 
11:   else
12:    return  $\tilde{\mathbf{A}}_i$ 
13:   end if
14: end while

```

---

The first key step of Algorithm 1 is line 4, where we compute the gradient of the principal’s utility function with respect to  $\tilde{\mathbf{A}}$ . This gradient involves terms that do not have an explicit functional form in terms of the decision variable, and we deal with each of these in turn.

First, consider the gradient of the normalized cut  $\phi(\mathcal{S})$  w.r.t.  $\tilde{\mathbf{A}}$ . Let  $\mathbf{x}_{\mathcal{S}}$  be the characteristic vector of  $\mathcal{S}$ , that is  $x_{\mathcal{S}}[i] = 1$  iff  $i \in \mathcal{S}$ . Let  $\tilde{\mathbf{D}}$  be the diagonal degree matrix  $\tilde{D}_{ii} = \sum_j \tilde{A}_{ij}$ , and let  $\tilde{\mathbf{L}} = \tilde{\mathbf{A}} - \tilde{\mathbf{D}}$  be the Laplacian matrix. Using  $\tilde{\mathbf{D}}$  and  $\tilde{\mathbf{L}}$  to express  $\text{vol}(\mathcal{S})$  and  $\text{cut}(\mathcal{S}, \mathcal{S}')$ , respectively, we have:

$$\phi(\mathcal{S}) = \mathbf{x}_{\mathcal{S}}^{\top} \tilde{\mathbf{L}} \mathbf{x}_{\mathcal{S}} \left( \frac{1}{\mathbf{x}_{\mathcal{S}}^{\top} \tilde{\mathbf{D}} \mathbf{x}_{\mathcal{S}}} + \frac{1}{\mathbf{x}_{\mathcal{S}'}^{\top} \tilde{\mathbf{D}} \mathbf{x}_{\mathcal{S}'}} \right). \quad (7)$$

It is clear that Eq. (7) is a differentiable function of  $\tilde{\mathbf{A}}$ . Computing its gradient  $\nabla_{\tilde{\mathbf{A}}} \phi(\mathcal{S})$  can then be handled by automatic differentiation tools such as PyTorch [26].

Next, we compute the gradient of  $\lambda_1(\tilde{\mathbf{A}}_{\mathcal{S}})$  w.r.t.  $\tilde{\mathbf{A}}$ . A standard way to compute  $\lambda_1(\tilde{\mathbf{A}}_{\mathcal{S}})$  is by using SVD. However, this is both prohibitively expensive ( $O(n^3)$ ), and does not provide us with the necessary gradient information. Instead, we use the power method [11] to compute  $\lambda_1(\tilde{\mathbf{A}}_{\mathcal{S}})$ . Let  $\mathbf{v}_{\mathcal{S}}$  be the eigenvector associated with the largest eigenvalue  $\lambda_1(\tilde{\mathbf{A}}_{\mathcal{S}})$ . Using Rayleigh quotients [34], we can compute  $\lambda_1(\tilde{\mathbf{A}}_{\mathcal{S}})$  as follows:

$$\mathbf{v}_{\mathcal{S}} = \arg \max_{\|\mathbf{x}\|_2=1} \mathbf{x}^{\top} \tilde{\mathbf{A}}_{\mathcal{S}} \mathbf{x} \quad (8a)$$

$$\lambda_1(\tilde{\mathbf{A}}_{\mathcal{S}}) = \mathbf{v}_{\mathcal{S}}^{\top} \tilde{\mathbf{A}}_{\mathcal{S}} \mathbf{v}_{\mathcal{S}}. \quad (8b)$$

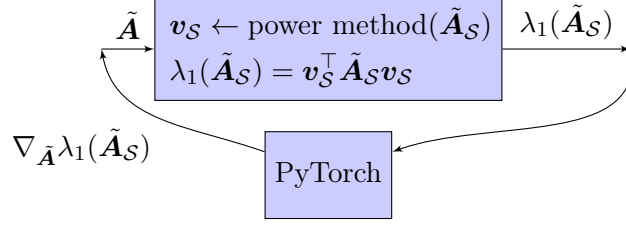


Figure 1: Computing  $\lambda_1(\tilde{\mathbf{A}}_{\mathcal{S}})$  given  $\tilde{\mathbf{A}}$ , which defines a differentiable function relation between  $\lambda_1(\tilde{\mathbf{A}}_{\mathcal{S}})$  and  $\tilde{\mathbf{A}}$ .

Thus, when  $\mathbf{v}_{\mathcal{S}}$  is known, the computation of  $\lambda_1(\tilde{\mathbf{A}}_{\mathcal{S}})$  reduces to matrix multiplications. In addition,  $\tilde{\mathbf{A}}_{\mathcal{S}}$  is usually sparse, so we can leverage sparse matrix multiplication to speed up the computation.

The remaining challenge is that  $\mathbf{v}_{\mathcal{S}}$  is an optimal solution of an optimization problem, and we need an explicit derivative of it. Fortunately, our problem has a special structure that we exploit to obtain an approximation of the derivative of  $\mathbf{v}_{\mathcal{S}}$ . From our experiments we find that  $\tilde{\mathbf{G}}_{\mathcal{S}}$  is nearly always connected. This means that the largest eigenvalue of  $\tilde{\mathbf{A}}_{\mathcal{S}}$  is simple. In addition, due to the Perron–Frobenius theorem, the absolute value of the largest eigenvalue is strictly greater than the absolute values of others, i.e.,  $|\lambda_1(\tilde{\mathbf{A}}_{\mathcal{S}})| > |\lambda_k(\tilde{\mathbf{A}}_{\mathcal{S}})|$  for all  $k \neq 1$ . Under these conditions, we can use the power method to estimate  $\mathbf{v}_{\mathcal{S}}$  by repeating the formula:  $\tilde{\mathbf{v}}_{\mathcal{S}}^{(t+1)} = \tilde{\mathbf{A}}_{\mathcal{S}} \tilde{\mathbf{v}}_{\mathcal{S}}^{(t)} / \|\tilde{\mathbf{A}}_{\mathcal{S}} \tilde{\mathbf{v}}_{\mathcal{S}}^{(t)}\|_2$ . The  $\ell_2$ -norm distance between  $\tilde{\mathbf{v}}_{\mathcal{S}}^k$  and  $\mathbf{v}_{\mathcal{S}}$  decreases in a rate  $O(\rho^k)$  [11], where  $\rho < 1$ . In our experiments we found  $k = 50$  is enough to give a high-quality estimation for a graph with 986 nodes. Intuitively, we are using a sequence of differentiable operations to approximate the argmax operation. Therefore the computation of  $\nabla_{\tilde{\mathbf{A}}} \lambda_1(\tilde{\mathbf{A}}_{\mathcal{S}})$  can be handled by PyTorch (see Figure 1).

We use the same machinery to compute  $\nabla_{\tilde{\mathbf{A}}} \sigma(\mathcal{S})$ . First, we write  $\sigma(\mathcal{S})$  in matrix notation:

$$\sigma(\mathcal{S}) = \mathbf{v}^{\top} \mathbf{x}_{\mathcal{S}}, \quad (9)$$

where  $\mathbf{v}$  is the unit eigenvector associated with  $\lambda_1(\tilde{\mathbf{A}})$ . Then we apply the power method to compute  $\mathbf{v}$ . Finally,  $\sigma(\mathcal{S})$  is just a linear function of  $\mathbf{v}$ . All of these operations are differentiable, and the computation of  $\nabla_{\tilde{\mathbf{A}}} \sigma(\mathcal{S})$  is handled by PyTorch.

The next issue addressed by the algorithm is the challenge imposed by the constraints involving preservation of the graph spectrum, which can result in a computationally challenging projection step which can also significantly harm solution quality. We address this challenge as follows. Given a real symmetric matrix  $\mathbf{X}$ , let  $\|\mathbf{X}\|_2$  denote its spectral norm. To satisfy Eq. (5), we use the following result from pseudospectrum theory (see [35], Theorem 2.2):

$$|\lambda_i(\tilde{\mathbf{A}}) - \lambda_i(\mathbf{A})| \leq \epsilon, i = 1, \dots, n \iff \|\tilde{\mathbf{A}} - \mathbf{A}\|_2 \leq \epsilon \quad (10)$$

Since  $\mathbf{\Delta} = \tilde{\mathbf{A}} - \mathbf{A}$  is a real symmetric matrix, we have  $\|\mathbf{\Delta}\|_2 = \max\{|\lambda_1(\mathbf{\Delta})|, |\lambda_n(\mathbf{\Delta})|\}$ . In addition, the eigen-decomposition of  $\mathbf{\Delta}$  indicates that  $-\lambda_n(\mathbf{\Delta}) = \lambda_1(-\mathbf{\Delta})$ , which leads to:

$$\tilde{\mathbf{A}} \text{ satisfies Eq. (5)} \iff \max\{|\lambda_1(\mathbf{\Delta})|, |\lambda_1(-\mathbf{\Delta})|\} \leq \epsilon. \quad (11)$$

This equivalence allows the principal to check whether she is within budget simply by evaluating  $\max\{|\lambda_1(\mathbf{\Delta})|, |\lambda_1(-\mathbf{\Delta})|\}$ , i.e., computing the largest eigenvalue of a real symmetric matrix, which can be computed efficiently using, e.g., the power method [11].

Our algorithm leverages this connection as follows. Line 9 in Algorithm 1 is a one step look-ahead, which ensures that the perturbation  $\Delta_i$  is only added to  $\tilde{\mathbf{A}}_i$  when there is enough budget. Recall from Section 2.2 that  $\|\Delta_i\|_2 = \max\{|\lambda_1(\Delta_i)|, |\lambda_1(-\Delta_i)|\}$ . Thus this step requires us to compute  $\lambda_1(\Delta_i)$  and  $\lambda_1(-\Delta_i)$ , using again the power method. Line 10 tracks the amount of budget used so far. We now show that the output of Algorithm 1 always returns a feasible solution. Suppose Algorithm 1 terminates after  $k > 1$  iterations. This means  $B_k + \|\eta_k \Delta_k\|_2 > \epsilon$  and  $B_k \leq \epsilon$ . In other words  $B_k = \sum_{i=1}^{k-1} \|\eta_i \Delta_i\|_2 \leq \epsilon$ . Note that the total amount of perturbation added to  $\mathbf{A}$  is  $\Delta = \sum_{i=1}^{k-1} \eta_i \Delta_i$ . The triangle inequality implies  $\|\Delta\|_2 \leq \epsilon$ .

For each iteration of Algorithm 1, the most expensive part comes from the power method and matrix multiplications. Let  $m$  be the number of nonzeros in  $\tilde{\mathbf{A}}_i$ ; if the graph is unweighted then  $m$  is the number of edges at this iteration. By leveraging the sparseness exhibited in  $\tilde{\mathbf{A}}_i$ , the power method runs in  $O(m)$  and the matrix multiplications cost  $O(mn)$ . Thus, the time complexity of each iteration is  $O(mn)$ .

Recall that our model for targeted diffusion is applicable to both weighted and unweighted graphs. For weighted graphs, the principal modifies the weights on existing edges. For unweighted graphs, the principal adds new edges or deletes existing edges from the graph. The main difference between the two settings is that the latter needs a rounding heuristic to convert a matrix with fractional entries to a binary adjacency matrix. We discuss this heuristic below.

After running Algorithm 1, we obtain a perturbed matrix  $\tilde{\mathbf{A}}$  with fractional entries. For unweighted graphs, a rounding heuristic is needed to convert  $\tilde{\mathbf{A}}$  to a valid adjacency matrix. Let  $\mathcal{D} = \{(i, j) | \tilde{A}_{i,j} \neq A_{i,j}\}$  be the set of candidate edges that will be added or deleted from  $G$ . For each edge  $(i, j) \in \mathcal{D}$  define the score  $s_{(i,j)} = |\tilde{A}_{i,j} - A_{i,j}|$ . Intuitively,  $s_{(i,j)}$  indicates the impact that adding or deleting the edge has on the principal's utility. Next, we iteratively modify  $G$ , by adding or deleting edges in  $\mathcal{D}$ , starting with the one with the largest  $s_{(i,j)}$ . The modification process stops when the budget is exhausted, which results in the desired binary adjacency matrix. For weighted graphs, let  $C = \max_{i,j} A_{ij}$  and normalize each entry by  $C$ , that is  $A_{ij}/C$ . We run Algorithm 1 on the normalized adjacency matrix, which results in  $\tilde{\mathbf{A}}$ . The desired adjacency matrix is obtained by multiplying each  $\tilde{A}_{ij}$  by  $C$ ,  $C\tilde{A}_{ij}$ . If integer weights are desired, a final rounding step is applied. Our experimental results show that the rounding heuristic is effective in practice.

## 4 Certified Robustness

This section addresses the following question: what are the limits on the principal's ability to successfully accomplish her attack? More precisely, we now seek to identify necessary conditions on the attack budget  $\epsilon$  so the attack succeeds; conversely, we can view a given graph to be *certified* to be robust to attacks that use a smaller budget than the one required.

Let  $\text{TargetDiff}(\mathcal{S}, G, \epsilon)$  be an instance of the targeted diffusion problem with targeted subset  $\mathcal{S}$ , underlying graph  $G$  and budget  $\epsilon$ . An instance  $\text{TargetDiff}(\mathcal{S}, G, \epsilon)$  can be successfully attacked if the principal is able to modify  $G$  into  $\tilde{G}$  (within budget  $\epsilon$ ) such that  $I(\tilde{G}_{\mathcal{S}}) - I(G_{\mathcal{S}}) > 0$ . Next we derive a necessary condition for successful targeted attacks, in the form of a lower bound on  $\epsilon$ .

In order to derive the necessary condition on  $\epsilon$ , we make use of our experimental observation that in successful attacks the degrees of nodes in the targeted subgraph  $G_{\mathcal{S}}$  always increase. This aligns well with intuition: a denser subgraph  $G_{\mathcal{S}}$  will tend to increase the propensity of the diffusion (e.g., of malware or treatment) to spread within it, which is one of our explicit objectives. Let  $d_i$  (resp.  $\tilde{d}_i$ ) be the degree of node  $i$  before (resp. after) graph modification. We assume if an

attack is successful, the degrees of nodes in  $G_{\mathcal{S}}$  are increased, i.e.,  $\tilde{d}_i \geq d_i$  for  $i \in \mathcal{S}$ .

Now, observe that computing the exact value of  $I(G_{\mathcal{S}})$  is intractable, since the exact computation of  $\pi_i$  is prohibitive (see, e.g., [36], Section IV.B). Van Mieghem et al. [36] proposed a simple yet effective estimator for  $\pi_i$  to be  $1 - \delta/(\beta d_i)$ . The estimator works in the regime  $\delta/\beta \leq d_{min}$ , where  $d_{min}$  is the minimum degree of  $G$ . Consequently, an estimator for  $I(G_{\mathcal{S}})$  is  $\hat{I}(G_{\mathcal{S}}) = \sum_{i \in \mathcal{S}} 1 - \delta/(\beta d_i)$ . We focus on the setting where the estimation error is bounded by a small number, i.e.,  $|\hat{I}(G_{\mathcal{S}}) - I(G_{\mathcal{S}})| \leq \tau$ . Note that  $\tau$  can be estimated from historical diffusion data. The formal statement of the necessary condition is in Theorem 1. Due to space limitation the proof is deferred to Appendix 3.

**Theorem 1.** *Given an instance `TargetDiff`( $\mathcal{S}, G, \epsilon$ ),  $I(G_{\mathcal{S}})$  is estimated by  $\hat{I}(G_{\mathcal{S}}) = \sum_{i \in \mathcal{S}} 1 - \delta/(\beta d_i)$ . Suppose the estimation error is bounded by  $\tau$ , i.e.,  $|\hat{I}(G_{\mathcal{S}}) - I(G_{\mathcal{S}})| \leq \tau$ , the degrees of nodes in  $\mathcal{S}$  are increased, i.e.,  $\tilde{d}_i \geq d_i$  for  $i \in \mathcal{S}$ , and  $\delta/\beta \leq d_{min}$ . In order to have  $I(G_{\tilde{\mathcal{S}}}) - I(G_{\mathcal{S}}) > 2\tau$ , the budget  $\epsilon$  must satisfy:*

$$\epsilon \geq \sqrt{\frac{|\mathcal{S}|}{n}} \left( \frac{\sum_{i \in \mathcal{S}} d_i^2}{|\mathcal{S}|} - \frac{(\sum_{i \in \mathcal{S}} d_i)^2}{|\mathcal{S}|^2} \right)^{1/2}. \quad (12)$$

The quantity inside the square root is always nonnegative due to Jensen’s inequality. The lower bound involves only structural properties of the graph (node degrees and the size of  $\mathcal{S}$ ) and thus can be easily computed given an arbitrary graph. As mentioned above, we can view this lower as a robustness certificate, or guarantee for the given graph. It guarantees, in particular, that when the budget is below the lower bound, the total probability of “infection” (e.g., malware infection) in  $G_{\mathcal{S}}$  cannot be increased by more than  $2\tau$ . In the special case of perfect estimation ( $\tau = 0$ ), it implies impossibility of increasing the susceptibility of  $G_{\mathcal{S}}$  to targeted diffusion.

The proof of Theorem 1 does not depend on the specific objective function proposed in this paper. Consequently, the certificate is not specific to our particular objective function. Further, the lower bound is independent of the parameters of the diffusion, i.e., the values of  $\delta$  and  $\beta$ , as long as  $\delta/\beta \leq d_{min}$ . In other words, it applies to both highly infectious (small  $\delta/\beta$ ) and slow-spreading (large  $\delta/\beta$ ) diffusion.

We briefly discuss the settings where the robustness guarantee is most applicable. First, the estimation for the infected ratio on  $G_{\mathcal{S}}$  is accurate, i.e.,  $|\hat{I}(G_{\mathcal{S}}) - I(G_{\mathcal{S}})| \leq \tau$  and  $\tau$  is small. According to Van Mieghem et al. [36], this usually happens on graphs with small degree variation. Another setting is where the degrees of nodes in  $G_{\mathcal{S}}$  increase as a result of the attack, which is both natural and empirically founded, as we mentioned earlier. Experimental results on synthetic networks to verify the robustness guarantee are presented in Appendix 6.

## 5 Experiments and Discussion

This section presents experimental results on three real-world datasets: an email network, an airport network, and a brain network. Additional results on synthetic networks can be found in Appendix 4.

For each network we run four experiments which differ in the hyper-parameters  $(\alpha_1, \alpha_2, \alpha_3)$ , corresponding to the four columns of Figure 2. The first uses  $\alpha_1 = \alpha_2 = \alpha_3 = 1/3$ , which encodes that the principal’s objectives are equally important. This is to show the overall effectiveness of our approach. The other three experiments are designed to show the effectiveness of each term in the principal’s objective function. For example, in the second experiment, we use hyper-parameters  $\alpha_1 = 1/3, \alpha_2 = 0$ , and  $\alpha_3 = 1/3$  (the hyper-parameters do not need to sum to one). To study



how the principal’s effectiveness changes with respect to her budget, we define a parameter  $\gamma$  that ranges from 10% to 50%. The budget is then set to  $\epsilon = \gamma \lambda_1(\mathbf{A})$ . A single initially infected node is selected uniformly at random.

Recall that we use  $G$  and  $\tilde{G}$  to denote the original and the modified graphs, respectively. We simulate the spreading dynamics 2000 times on both  $G$  and  $\tilde{G}$ . For unweighted graphs the recovery rate  $\delta$  and transmission rate  $\beta$  are set to 0.24 and 0.06, respectively, while for weighted graphs  $\delta = 0.24$  and  $\beta = 0.2$ . Additional experimental results for other values of  $\delta$  and  $\beta$  are in Appendix 5. The spreading dynamics converges exponentially fast to the steady state: empirically, we found 30 time steps to be enough to reach the steady state in most cases.<sup>4</sup> When the simulation finishes, we extract the number of nodes that are “infected”. We use  $I_{\text{original}}$  and  $I_{\text{modified}}$  to represent the fractions of infected nodes on  $G$  and  $\tilde{G}$ , respectively.

**Unweighted Graphs:** We consider an email network [18]. The largest connected component of the network is extracted as  $G$ , which has 986 nodes. An edge  $(i, j)$  indicates that there were email exchanges between nodes  $i$  and  $j$ . This data set contains ground-truth labels to indicate which community a node belongs to. We uniformly at random pick a community with 15 nodes as  $\mathcal{S}$ .

The experimental results for the email network are at the top row of Figure 2. The overall effectiveness of our approach is shown in the first column. The difference of the impact on the modified and original graphs, that is  $I_{\text{modified}} - I_{\text{original}}$ , is shown for  $G_{\mathcal{S}}$  (blue line) and  $G_{\mathcal{S}'}$  (orange line), respectively. As  $\gamma$  gets larger, the impact on  $G_{\mathcal{S}}$  (blue line) increases, while the impact on  $G_{\mathcal{S}'}$  (orange line) is under control, which demonstrates that the proposed approach is highly effective at both increasing the impact of diffusion on the targeted subgraph, and at the same time preventing the impact on the remaining graph.

The second column is to show that maximizing  $\lambda_1(\tilde{\mathbf{A}}_{\mathcal{S}})$  leads to higher infected ratios. The labels of the  $y$ -axis become  $I_{\text{modified}}^{\mathcal{S}} - I_{\text{original}}^{\mathcal{S}}$ , which highlights that the infected ratios are for the targeted subgraph  $G_{\mathcal{S}}$  (the higher the better). Note that  $\alpha_2$  is set to zero in order to avoid the coupling between the eigenvector centrality of  $\mathcal{S}$  and  $\lambda_1(\tilde{\mathbf{A}}_{\mathcal{S}})$ . From the plot it is clear that maximizing  $\lambda_1(\tilde{\mathbf{A}}_{\mathcal{S}})$  is important to increase the infected ratios within  $G_{\mathcal{S}}$  (the blue line). Note that solely maximizing the normalized cut of  $\mathcal{S}$  may backfire (the red line), as a large portion of edges are deleted from  $G_{\mathcal{S}}$  when  $\gamma$  increases.

The third column is to show the effectiveness of limiting the impact on  $G_{\mathcal{S}'}$  by maximizing the eigenvector centrality of  $\mathcal{S}$ . The  $y$ -axis represents  $I_{\text{modified}}^{\mathcal{S}'} - I_{\text{original}}^{\mathcal{S}'}$ , which highlights that the infected ratios are for the non-targeted subgraph  $G_{\mathcal{S}'}$  (the lower the better). The plot shows that the impact on  $G_{\mathcal{S}'}$  is well limited; the effectiveness is most significant when  $\gamma > 40\%$ .

The last column is to show the effectiveness of maximizing the normalized cut of  $\mathcal{S}$ . We set  $\alpha_2 = 0$  to avoid the effect of maximizing the eigenvector centrality of  $\mathcal{S}$ . Observe that maximizing the normalized cut of  $\mathcal{S}$  is effective in increasing the infected ratio within  $G_{\mathcal{S}}$ .

---

<sup>4</sup>The SIS model is similar to an irreducible ( $G$  and  $\tilde{G}$  are connected) and aperiodic (each infected node recovers with probability  $\delta$ ) Markov chain representing a lazy random walk on the network.

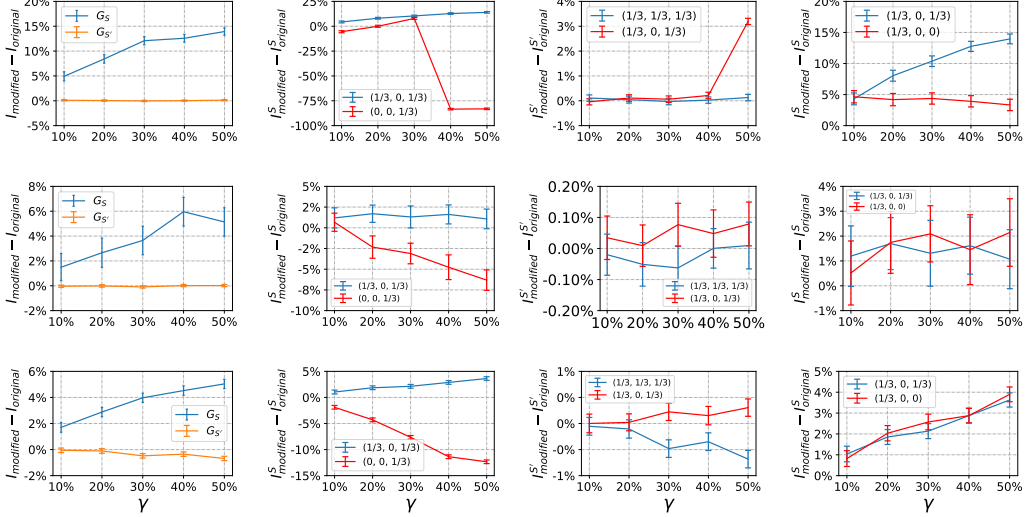


Figure 2: Experiments to show the effectiveness of the model. **Top**: the email network; **Middle**: the airport network; **Bottom**: the brain network. The first column shows the overall effectiveness of the model. The remaining three columns (from left to right) show the effectiveness of: 1) maximizing  $\lambda_1(\tilde{A}_S)$ ; 2) Maximizing the eigenvector centrality of  $\mathcal{S}$ ; 3) maximizing the normalized cut of  $\mathcal{S}$ .

**Weighted Graphs:** We consider an airport network and a brain network. The airport network [24] was collected from the website of Bureau of Transportation Statistics of the U.S., where the nodes represent all of the 1572 airports in the U.S. and the weights on edges encode the number of passengers traveled between two airports in 2010. We scaled the weights on the airport network to  $[0, 1]$ . The targeted set  $\mathcal{S}$  was chosen by first sampling a node  $i$  uniformly at random, and then setting  $\mathcal{S}$  to be  $i$  and all its neighbors. We report experimental results for an  $\mathcal{S}$  with 60 nodes. The brain network [8] consists of 638 nodes where each node corresponds to a region in human brain. An edge between nodes  $i$  and  $j$  indicates that the two regions have co-activated on some tasks. The weight on the edge quantifies the strength of the co-activation estimated by the Jaccard index. The weights on edges lie in  $[0, 1]$ . The 638 regions are categorized into four areas: default mode, visual, fronto-parietal, and central. Each area is responsible for some functionality of human. We select 100 nodes from the central area as the targeted set  $\mathcal{S}$ .

The results for the airport (resp. brain) network are at the middle (resp. bottom) row of Figure 2. The overall trend is similar to that of the email network, except that maximizing the normalized cut of  $\mathcal{S}$  is not effective in increasing the infected ratio within  $G_S$ . This suggests that on weighted graphs normalized cut might not be a good heuristic to increase the centrality of  $\mathcal{S}$ .

**Final Word:** Our experiments show that our model and optimization algorithm are effective in implementing targeted diffusions on real-world graphs. The algorithm leverages Rayleigh quotients and pseudospectrum theory, which is scalable to large graphs. We also derived a necessary condition to certify whether a network is robust against a broad class of targeted diffusion.

## References

- [1] Victor Amelkin and Ambuj K Singh. Fighting opinion control in social networks via link recommendation. In *Proceedings of the 25th ACM SIGKDD international conference on Knowledge discovery and data mining*, pages 677–685, 2019.

- [2] Konstantin Avrachenkov and Nelly Litvak. The effect of new links on google pagerank. *Stochastic Models*, 22(2):319–331, 2006.
- [3] Norman TJ Bailey et al. *The mathematical theory of infectious diseases and its applications*. Charles Griffin & Company Ltd, 1975.
- [4] Albert-László Barabási and Réka Albert. Emergence of scaling in random networks. *science*, 286(5439):509–512, 1999.
- [5] Deepayan Chakrabarti, Yang Wang, Chenxi Wang, Jurij Leskovec, and Christos Faloutsos. Epidemic thresholds in real networks. *ACM Transactions on Information and System Security (TISSEC)*, 10(4):1–26, 2008.
- [6] Chen Chen, Hanghang Tong, B. Aditya Prakash, Charalampos E. Tsourakakis, Tina Eliassi-Rad, Christos Faloutsos, and Duen Horng Chau. Node immunization on large graphs: Theory and algorithms. *IEEE Transactions on Knowledge and Data Engineering*, 28(1):113–126, 2016.
- [7] Wei Chen, Yajun Wang, and Siyu Yang. Efficient influence maximization in social networks. In *Proceedings of the 15th ACM SIGKDD international conference on Knowledge discovery and data mining*, pages 199–208, 2009.
- [8] Nicolas A Crossley, Andrea Mechelli, Petra E Vértes, Toby T Winton-Brown, Ameera X Patel, Cedric E Ginestet, Philip McGuire, and Edward T Bullmore. Cognitive relevance of the community structure of the human brain functional coactivation network. *Proceedings of the National Academy of Sciences*, 110(28):11583–11588, 2013.
- [9] Ernesto Estrada. ‘hubs-repelling’ laplacian and related diffusion on graphs/networks. *Linear Algebra and its Applications*, 2020.
- [10] Pablo Fleurquin, José J Ramasco, and Victor M Eguiluz. Systemic delay propagation in the us airport network. *Scientific reports*, 3:1159, 2013.
- [11] Gene Golub and Charles Van Loan. *Matrix computations*. Johns Hopkins Studies in Mathematical Sciences, 1996.
- [12] Nika Haghtalab, Aron Laszka, Ariel D. Procaccia, Yevgeniy Vorobeychik, and Xenofon Koutsoukos. Monitoring stealthy diffusions. *Knowledge and Information Systems*, 2017.
- [13] Christopher Ho, Mykel J Kochenderfer, Vineet Mehta, and Rajmonda S Caceres. Control of epidemics on graphs. In *54th IEEE Conference on Decision and Control (CDC)*, pages 4202–4207. IEEE, 2015.
- [14] David Kempe, Jon Kleinberg, and Éva Tardos. Maximizing the spread of influence through a social network. In *Proceedings of the ninth ACM SIGKDD international conference on Knowledge discovery and data mining*, pages 137–146, 2003.
- [15] David Kempe, Sixie Yu, and Yevgeniy Vorobeychik. Inducing equilibria in networked public goods games through network structure modification. In *Proceedings of the 19th International Conference on Autonomous Agents and MultiAgent Systems*, 2020.
- [16] Long T Le, Tina Eliassi-Rad, and Hanghang Tong. Met: A fast algorithm for minimizing propagation in large graphs with small eigen-gaps. In *Proceedings of the 2015 SIAM International Conference on Data Mining*, pages 694–702. SIAM, 2015.
- [17] Stamatios Lefkimiatis, John Paul Ward, and Michael Unser. Hessian Schatten-norm regularization for linear inverse problems. *IEEE transactions on image processing*, 22(5): 1873–1888, 2013.

- [18] Jure Leskovec, Jon Kleinberg, and Christos Faloutsos. Graph evolution: Densification and shrinking diameters. *ACM transactions on Knowledge Discovery from Data (TKDD)*, 1(1): 2–es, 2007.
- [19] Jure Leskovec, Mary McGlohon, Christos Faloutsos, Natalie Glance, and Matthew Hurst. Patterns of cascading behavior in large blog graphs. In *Proceedings of the 2007 SIAM international conference on data mining*, pages 551–556. SIAM, 2007.
- [20] Jure Leskovec, Lars Backstrom, and Jon Kleinberg. Meme-tracking and the dynamics of the news cycle. In *Proceedings of the 15th ACM SIGKDD international conference on Knowledge discovery and data mining*, pages 497–506, 2009.
- [21] Marina Meila and Jianbo Shi. Learning segmentation by random walks. In *Advances in neural information processing systems*, pages 873–879, 2001.
- [22] Flaviano Morone and Hernán A Makse. Influence maximization in complex networks through optimal percolation. *Nature*, 524(7563):65, 2015.
- [23] Adilson E Motter and Ying-Cheng Lai. Cascade-based attacks on complex networks. *Physical Review E*, 66(6):065102, 2002.
- [24] Tore Opsahl. U.s. airport network traffic data in 2010. <https://toreopsahl.com/2011/08/12/why-anchorage-is-not-that-important-binary-ties-and-sample-selection/>, 2010.
- [25] Romualdo Pastor-Satorras, Claudio Castellano, Piet Van Mieghem, and Alessandro Vespignani. Epidemic processes in complex networks. *Reviews of modern physics*, 87(3):925, 2015.
- [26] Adam Paszke, Sam Gross, Soumith Chintala, Gregory Chanan, Edward Yang, Zachary DeVito, Zeming Lin, Alban Desmaison, Luca Antiga, and Adam Lerer. Automatic differentiation in pytorch, 2017.
- [27] B Aditya Prakash, Deepayan Chakrabarti, Nicholas C Valler, Michalis Faloutsos, and Christos Faloutsos. Threshold conditions for arbitrary cascade models on arbitrary networks. *Knowledge and information systems*, 33(3):549–575, 2012.
- [28] Victor M Preciado, Michael Zargham, Chinwendu Enyioha, Ali Jadbabaie, and George Pappas. Optimal vaccine allocation to control epidemic outbreaks in arbitrary networks. In *52nd IEEE Conference on Decision and Control (CDC)*, pages 7486–7491. IEEE, 2013.
- [29] Sudip Saha, Abhijin Adiga, B Aditya Prakash, and Anil Kumar S Vullikanti. Approximation algorithms for reducing the spectral radius to control epidemic spread. In *Proceedings of the 2015 SIAM International Conference on Data Mining*, pages 568–576. SIAM, 2015.
- [30] Comandur Seshadhri, Tamara G Kolda, and Ali Pinar. Community structure and scale-free collections of erdős-rényi graphs. *Physical Review E*, 85(5):056109, 2012.
- [31] Hanghang Tong, B Aditya Prakash, Charalampos Tsourakakis, Tina Eliassi-Rad, Christos Faloutsos, and Duen Horng Chau. On the vulnerability of large graphs. In *2010 IEEE International Conference on Data Mining*, pages 1091–1096. IEEE, 2010.
- [32] Hanghang Tong, B Aditya Prakash, Tina Eliassi-Rad, Michalis Faloutsos, and Christos Faloutsos. Gelling, and melting, large graphs by edge manipulation. In *Proceedings of the 21st ACM international conference on Information and knowledge management*, pages 245–254, 2012.
- [33] Leo Torres, Kevin S Chan, Hanghang Tong, and Tina Eliassi-Rad. Node immunization with non-backtracking eigenvalues. *arXiv preprint arXiv:2002.12309*, 2020.

- [34] Lloyd N Trefethen and David Bau III. *Numerical linear algebra*, volume 50. SIAM, 1997.
- [35] Lloyd N Trefethen and Mark Embree. *Spectra and pseudospectra: the behavior of nonnormal matrices and operators*. Princeton University Press, 2005.
- [36] Piet Van Mieghem, Jasmina Omic, and Robert Kooij. Virus spread in networks. *IEEE/ACM Transactions On Networking*, 17(1):1–14, 2008.
- [37] Piet Van Mieghem, Dragan Stevanović, Fernando Kuipers, Cong Li, Ruud Van De Bovenkamp, Daijie Liu, and Huijuan Wang. Decreasing the spectral radius of a graph by link removals. *Physical Review E*, 84(1):016101, 2011.
- [38] Tan Van Vu and Yoshihiko Hasegawa. Diffusion-dynamics laws in stochastic reaction networks. *Physical Review E*, 99:012416, 2019.
- [39] Zhihui Wang and Thomas S. Deisboeck. Dynamic targeting in cancer treatment. *Frontiers in Physiology*, 10:1–9, 2019.
- [40] Duncan J Watts and Steven H Strogatz. Collective dynamics of small-world networks. *nature*, 393(6684):440, 1998.
- [41] Yang Yang, Takashi Nishikawa, and Adilson E Motter. Small vulnerable sets determine large network cascades in power grids. *Science*, 358(6365):eaan3184, 2017.
- [42] Sixie Yu and Yevgeniy Vorobeychik. Removing malicious nodes from networks. In *Proceedings of the 18th International Conference on Autonomous Agents and MultiAgent Systems*, pages 314–322. International Foundation for Autonomous Agents and Multiagent Systems, 2019.
- [43] Haifeng Zhang, Yevgeniy Vorobeychik, Joshua Letchford, and Kiran Lakkaraju. Data-driven agent-based modeling, with application to rooftop solar adoption. *Autonomous Agents and Multi-Agent Systems*, 30(6):1023–1049, 2016.
- [44] Kai Zhou, Tomasz P Michalak, Marcin Waniek, Talal Rahwan, and Yevgeniy Vorobeychik. Attacking similarity-based link prediction in social networks. In *Proceedings of the 18th International Conference on Autonomous Agents and MultiAgent Systems*, pages 305–313. International Foundation for Autonomous Agents and Multiagent Systems, 2019.

# Appendix

## 1 Generalization to Other Diffusion Dynamics

In this section we discuss generalization of the targeted diffusion model, i.e., Eq. (6), to other common diffusion dynamics. The fundamental question is: does the heuristic encoded by the model apply to other scenarios with different diffusion dynamics (e.g., SIR or SEIR)?

First, the feasible region of the model is independent of the diffusion dynamics, as it is only related to the spectral properties of the underlying graph. Thus, the structural (i.e., spectra, degree sequence, and triangle distribution) preserving properties of the diffusion model generalize to other diffusion dynamics. Next, recall that the objective function of the model is the following

$$\alpha_1 \lambda_1(\tilde{\mathbf{A}}_{\mathcal{S}}) + \alpha_2 \sigma(\mathcal{S}) + \alpha_3 \phi(\mathcal{S}).$$

The third term is the normalized cut, which only depends on structural properties of the underlying graph, so it generalizes to any other diffusion dynamics. The first term also generalizes to many common diffusion dynamics, including SIR and SEIR, as their epidemic thresholds are known to also be determined by the largest eigenvalue of the underlying adjacency matrix [27]. The only exception is the second term  $\sigma(\mathcal{S})$ , that is, limiting the impact on non-targeted subset through maximizing the eigencentality of the targeted subset. This is because the rationale of maximizing  $\sigma(\mathcal{S})$  depends on the steady state of the diffusion dynamics. Here, the steady state is where in the long run a constant (in average) fraction of infected nodes exist. However, both SIR and SEIR have been shown without a steady state, as in the long run all nodes will be in the recovered state (i.e., immune to the diffusion) [25].

Finally, the certified robustness in Section 4 generalizes to other diffusion dynamics, as its proof only depends on the spectral properties of the underlying graph.

## 2 Degree Sequence and Triangle

We now show that satisfying the restrictions Eq (5) implies that certain structural properties of the graph will be perturbed by only a small amount.

Indeed, the principal's action has mild impact on the degree sequence of  $G$ . Let  $\mathbf{d} = \mathbf{A}\mathbf{1}$  be the vector whose  $i$ -th entry is the degree of the  $i$ -th node in the original graph, and similarly, let  $\tilde{\mathbf{d}} = \tilde{\mathbf{A}}\mathbf{1}$  be the degree sequence after the perturbation.

**Proposition 2.** *The degree sequence of  $G$  before and after the perturbation satisfies:*

$$\|\tilde{\mathbf{d}} - \mathbf{d}\|_2 \leq \sqrt{n}\epsilon. \quad (13)$$

*Proof.*

$$\begin{aligned} \|\tilde{\mathbf{d}} - \mathbf{d}\|_2 &= \|\tilde{\mathbf{A}}\mathbf{1} - \mathbf{A}\mathbf{1}\|_2 \stackrel{(a)}{=} \|\mathbf{\Delta}\mathbf{1}\|_2 = \|\mathbf{\Delta}(1/\sqrt{n})\mathbf{1}\sqrt{n}\|_2 \\ &\leq \sqrt{n} \max_{\|x\|=1} \|\mathbf{\Delta}x\|_2 \\ &\stackrel{(b)}{=} \sqrt{n}\|\mathbf{\Delta}\|_2 \\ &\leq \sqrt{n}\epsilon, \end{aligned} \quad (14)$$

where (a) is due to the fact that  $\tilde{\mathbf{A}} - \mathbf{A} = \mathbf{\Delta}$ , and (b) comes from the definition of spectral norm.  $\square$

A direct corollary of Proposition 2 concerns the average degree of  $G$ .

**Corollary 3.** *The average degree of  $G$  after the perturbation is within  $\epsilon$  of the average degree before the perturbation:*

$$\left| d_{avg}(G; \tilde{\mathbf{A}}) - d_{avg}(G; \mathbf{A}) \right| \leq \epsilon. \quad (15)$$

*Proof.* Note that  $d_{avg}(\tilde{G}) = \frac{\mathbf{1}^\top \tilde{\mathbf{d}}}{n}$  and  $d_{avg}(G) = \frac{\mathbf{1}^\top \mathbf{d}}{n}$ . Thus we have:

$$\begin{aligned} \left| \mathbf{1}^\top \tilde{\mathbf{d}}/n - \mathbf{1}^\top \mathbf{d}/n \right| &= (1/n) \left| \mathbf{1}^\top (\tilde{\mathbf{d}} - \mathbf{d}) \right| \\ &\leq (1/n) \|\mathbf{1}\|_2 \cdot \|\tilde{\mathbf{d}} - \mathbf{d}\|_2 \\ &= \epsilon. \end{aligned} \quad (16)$$

□

Next, we perform a similar analysis for the number of triangles before and after the perturbation.

**Proposition 4.** *Assume  $G$  is unweighted with  $m$  edges and  $T$  triangles. Suppose the number of triangles after the perturbation is  $\tilde{T}$ . Then we have*

$$|T - \tilde{T}| \leq \epsilon m, \quad (17)$$

where the estimate is correct up to a first order approximation.

*Proof.* Since  $G$  is unweighted, we have  $T = \text{Tr}(\mathbf{A}^3)/6$ , where  $\text{Tr}$  is the trace operator. The restrictions Eq. (5) guarantee that we can write  $\lambda_i(\tilde{\mathbf{A}}) = \lambda_i(\mathbf{A}) + \eta_i \epsilon$ , where  $\eta_i \in [-1, 1]$ . Thus,

$$6\tilde{T} = \sum_i^n \lambda_i(\tilde{\mathbf{A}}^3) = \sum_i^n \lambda_i(\tilde{\mathbf{A}})^3 = \sum_i^n (\lambda_i(\mathbf{A}) + \eta_i \epsilon)^3. \quad (18)$$

Expanding the cube and neglecting the terms of higher order in  $\eta_i$ , we have

$$6\tilde{T} \approx \sum_i^n \lambda_i(\mathbf{A})^3 + 3\epsilon \sum_i^n \lambda_i(\mathbf{A})^2 \eta_i = 6T + 3\epsilon \sum_i^n \lambda_i(\mathbf{A})^2 \eta_i. \quad (19)$$

And thus

$$2|\tilde{T} - T| \approx \epsilon \left| \sum_i^n \lambda_i(\mathbf{A})^2 \eta_i \right| \leq \epsilon \sum_i^n |\lambda_i(\mathbf{A})^2 \eta_i| \leq \epsilon \sum_i^n \lambda_i(\mathbf{A})^2 = \epsilon \text{Tr}(\mathbf{A}^2). \quad (20)$$

Since  $\mathbf{A}$  is symmetric and binary, we have  $\text{Tr}(\mathbf{A}^2) = 2m$ , where  $m$  is the number of edges in  $G$ . □

In what follows we present experimental results to show that the spectra and degree sequences do not change a lot due to the targeted diffusion. The spectra and degree sequences of  $G$  and  $\tilde{G}$  are showed in Figure 3, in which the top row presents the spectra with the eigenvalues as ranked in descending order, and the bottom row presents the degree sequences. The three columns (from left to right) correspond to the email network, the airport network, and the brain network, respectively. The parameter  $\gamma$  is set to 0.5, the most powerful principal.

**The Email Network:** From Figure 3 (top row), the eigenvalues with large value admit the largest deviation, while the bottom row of that figure shows that the degree sequence is not significantly affected by the targeted diffusion. In fact, the change to the original degree sequence is mild, and a student's t-test cannot differentiate the modified degree sequence from the original one (p-value=0.081).

**The Airport and The Brain Networks:** The spectra and degree sequences of  $G$  and  $\tilde{G}$  are showed in the last two columns of Figure 3. As we can see from Figure 3 (top row), the graph spectrum is again nearly preserved, except the eigenvalues with small values admit some deviation. Similarly, the modified degree sequences cannot be differentiated from the original one by student's t-tests (airport: p-value=0.4969, brain: p-value=0.9919).

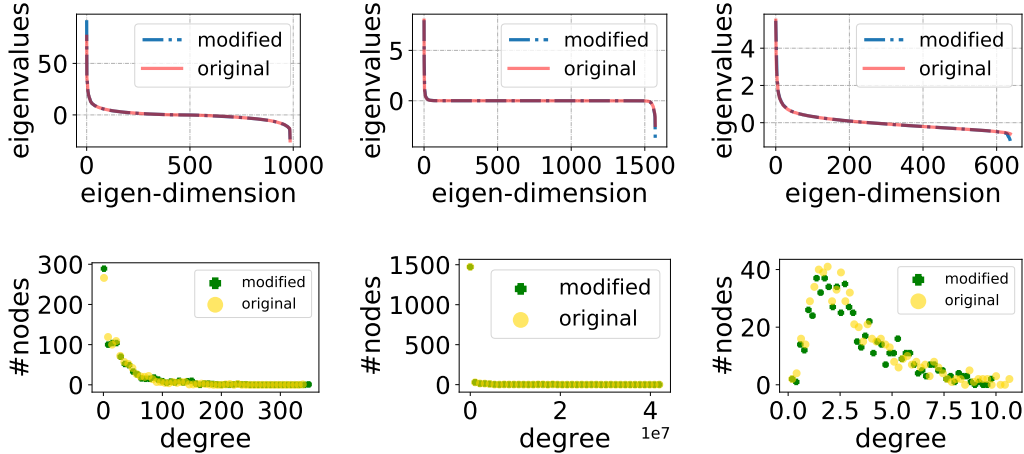


Figure 3: Spectra (top) and degree sequences (bottom) for the **left:** the email network; **middle:** the airport network; and **right:** the brain network. The hyper-parameters are set to  $\alpha_1 = \alpha_2 = \alpha_3 = 1/3$ .

### 3 Proof of Theorem 1

*Proof.* From the discussion in the main paper, an instance  $\text{TargetDiff}(\mathcal{S}, G, \epsilon)$  can be encoded by the following meta model:

$$\begin{aligned} \max_{\tilde{\mathbf{A}}} \quad & I(\tilde{G}_{\mathcal{S}}) - I(G_{\mathcal{S}}) \\ \text{s.t.} \quad & \tilde{\mathbf{A}} \in \mathcal{P}. \end{aligned} \tag{21}$$

As discussed in [36] (see Section IV.B), computing the exact value of  $I(G_{\mathcal{S}})$  is intractable, since the exact computation of  $\pi_i$  is challenging. Our model Eq. (6) can be thought of as a tractable proxy to the meta model. An estimation to  $I(G_{\mathcal{S}})$  is given in [36], i.e.,  $\hat{I}(G_{\mathcal{S}}) = \sum_{i \in \mathcal{S}} 1 - \delta/(\beta d_i)$ , where  $d_i$  is the degree of node  $i$  in  $G$ . The estimator works in the region  $\delta/\beta \leq d_{\min}$ , where  $d_{\min}$  is the minimum degree of  $G$ . When the estimation is reasonably good, that is  $|\hat{I}(G_{\mathcal{S}}) - I(G_{\mathcal{S}})| \leq \tau$ , we have the following relation:

$$I(\tilde{G}_{\mathcal{S}}) - I(G_{\mathcal{S}}) > 2\tau \implies (\hat{I}(\tilde{G}_{\mathcal{S}}) + \tau) - (\hat{I}(G_{\mathcal{S}}) - \tau) > 2\tau \implies \hat{I}(\tilde{G}_{\mathcal{S}}) - \hat{I}(G_{\mathcal{S}}) > 0.$$

Thus, in what follows we focus on deriving the necessary condition for  $\hat{I}(\tilde{G}_{\mathcal{S}}) - \hat{I}(G_{\mathcal{S}}) > 0$ , which directly translates to the necessary condition for  $I(\tilde{G}_{\mathcal{S}}) - I(G_{\mathcal{S}}) > 2\tau$ .

Suppose there exists an adjacency matrix  $\tilde{\mathbf{A}}^* \in \mathcal{P}$  such that  $I(\tilde{G}_{\mathcal{S}}) - I(G_{\mathcal{S}}) > 2\tau$ . This indicates that the corresponding instance  $\text{TargetDiff}(\mathcal{S}, G, \epsilon)$  is successful. Consequently, it follows that  $\hat{I}(\tilde{G}_{\mathcal{S}}) - \hat{I}(G_{\mathcal{S}}) > 0$ . Recall that  $\hat{I}(\tilde{G}_{\mathcal{S}}) - \hat{I}(G_{\mathcal{S}}) = \frac{\delta}{\beta} \sum_{i \in \mathcal{S}} (\frac{1}{\tilde{d}_i} - \frac{1}{d_i})$ . Let  $\tilde{\mathbf{d}}_{\mathcal{S}} \in \mathbb{R}^{|\mathcal{S}|}$  represent the degree sequence of nodes in  $\mathcal{S}$ . Due to Proposition 2 we have  $\|\tilde{\mathbf{d}}_{\mathcal{S}} - \mathbf{d}_{\mathcal{S}}\|_2^2 \leq \|\tilde{\mathbf{d}} - \mathbf{d}\|_2^2 \leq n\epsilon^2$ . Consider the optimization problem in Eq. (22), where the objective function is  $\hat{I}(\tilde{G}_{\mathcal{S}}) - \hat{I}(G_{\mathcal{S}})$  (up to a multiplicative factor). The last constraint follows from the assumption that for a successful



instance the degrees of nodes in  $\mathcal{S}$  increase. The fact that  $\hat{I}(\tilde{G}_{\mathcal{S}}) - \hat{I}(G_{\mathcal{S}}) > 0$  implies that the optimal solution of Eq. (22) exists and the associated objective value is greater than zero.

$$\begin{aligned} \max_{\tilde{\mathbf{d}}_{\mathcal{S}}} \quad & \sum_{i \in \mathcal{S}} \left( \frac{1}{d_i} - \frac{1}{\tilde{d}_i} \right) \\ \text{s.t.} \quad & \|\tilde{\mathbf{d}}_{\mathcal{S}} - \mathbf{d}_{\mathcal{S}}\|_2^2 \leq n\epsilon^2 \\ & \tilde{\mathbf{d}}_{\mathcal{S}} \succeq \mathbf{d}_{\mathcal{S}}. \end{aligned} \tag{22}$$

Denote the feasible region of the above optimization problem as  $\mathcal{M}$ . Note that  $\mathcal{M}$  is a convex set since it is the intersection of two convex sets.

The objective function is concave in  $\tilde{\mathbf{d}}_{\mathcal{S}}$ , since it is twice differentiable on the feasible region  $\mathcal{M}$  and the Hessian matrix is negative definite; the Hessian matrix is a diagonal matrix with the  $i$ -th diagonal element being  $-2/\tilde{d}_i^3$ . Thus, Eq. (22) is a convex optimization problem. Note that the Slater's condition is satisfied (e.g., with  $\tilde{\mathbf{d}}_{\mathcal{S}} = \mathbf{d}_{\mathcal{S}}$ ), which indicates that strong duality holds. Thus, the KKT conditions are satisfied at *any* primal and dual optimal solutions.

For convenience, in what follows we use  $d_i$  (resp.  $\tilde{d}_i$ ) to represent the degree of a node  $i \in \mathcal{S}$  before (resp. after) graph modification. The Lagrange function of Eq. (22) is:

$$\mathcal{L}(\tilde{\mathbf{d}}_{\mathcal{S}}, \lambda, \boldsymbol{\beta}) = \sum_{i \in \mathcal{S}} \left( \frac{1}{d_i} - \frac{1}{\tilde{d}_i} \right) + \lambda \left( n\epsilon^2 - \|\tilde{\mathbf{d}}_{\mathcal{S}} - \mathbf{d}_{\mathcal{S}}\|_2^2 \right) + \boldsymbol{\beta}^\top (\tilde{\mathbf{d}}_{\mathcal{S}} - \mathbf{d}_{\mathcal{S}}),$$

where  $\lambda \geq 0$  and  $\boldsymbol{\beta} \succeq \mathbf{0}$  are Lagrangian multipliers. Recall that the degrees of nodes in  $\mathcal{S}$  are increased, i.e.,  $\tilde{d}_i \geq d_i$  for all  $i \in \mathcal{S}$ . Note that for a node  $i \in \mathcal{S}$  such that  $\tilde{d}_i = d_i$ , we let the corresponding  $\beta_i = 0$ . Thus, by complementary slackness, we have  $\beta_i = 0$  for all  $i \in \mathcal{S}$ . The gradient of  $\mathcal{L}(\tilde{\mathbf{d}}_{\mathcal{S}}, \lambda, \boldsymbol{\beta})$  w.r.t.  $\tilde{d}_i$  becomes:

$$\frac{\partial \mathcal{L}}{\partial \tilde{d}_i} = \frac{1}{\tilde{d}_i^2} - 2\lambda\tilde{d}_i + \beta_i = \frac{1}{\tilde{d}_i^2} - 2\lambda\tilde{d}_i.$$

Setting the gradient to zero leads to:

$$\tilde{d}_i = \left( \frac{1}{2\lambda} \right)^{1/3}, \forall i \in \mathcal{S}.$$

Since the optimal solution exists, we have  $\lambda \neq 0$ . By complementary slackness we have  $\lambda \left( n\epsilon^2 - \|\tilde{\mathbf{d}}_{\mathcal{S}} - \mathbf{d}_{\mathcal{S}}\|_2^2 \right) = 0$ , which indicates:

$$n\epsilon^2 = \|\tilde{\mathbf{d}}_{\mathcal{S}} - \mathbf{d}_{\mathcal{S}}\|_2^2.$$

Expand the above equation:

$$n\epsilon^2 = \|\tilde{\mathbf{d}}_{\mathcal{S}} - \mathbf{d}_{\mathcal{S}}\|_2^2 \tag{23}$$

$$= \sum_{i \in \mathcal{S}} (\tilde{d}_i - d_i)^2 \tag{24}$$

$$= \sum_{i \in \mathcal{S}} \left( \left( \frac{1}{2\lambda} \right)^{1/3} - d_i \right)^2. \tag{25}$$

Substitute  $\left( \frac{1}{2\lambda} \right)^{1/3}$  with a variable  $x$  and re-arrange the above equation:

$$x^2 - \frac{2 \sum_{i \in \mathcal{S}} d_i}{|\mathcal{S}|} x + \frac{\sum_{i \in \mathcal{S}} d_i^2 - n\epsilon^2}{|\mathcal{S}|} = 0.$$

According to vieta theorem, a necessary condition that we can solve for  $x \in \mathbb{R}$  from the above equation is:

$$\left(\frac{2\sum_{i \in \mathcal{S}} d_i}{|\mathcal{S}|}\right)^2 - 4\left(\frac{\sum_{i \in \mathcal{S}} d_i^2 - n\epsilon^2}{|\mathcal{S}|}\right) \geq 0,$$

which leads to:

$$\epsilon \geq \sqrt{\frac{|\mathcal{S}|}{n}} \left( \frac{\sum_{i \in \mathcal{S}} d_i^2}{|\mathcal{S}|} - \frac{(\sum_{i \in \mathcal{S}} d_i)^2}{|\mathcal{S}|^2} \right)^{1/2}.$$

□

## 4 Additional Results on Synthetic Networks

In this section we show experimental results on synthetic unweighted graphs with 375 nodes. We focus on three classes of networks: Barabasi-Albert (BA), Small-World, and BTER [30]. BA is characterized by its power-law degree distribution [4]. Small-World is well-known for its local clustering in a way as to qualitatively resemble real networks [40]. BTER are generative network models that can be calibrated to match real-world networks, in particular, to reproduce the community structures [30].

The experimental setup is similar to the setup for the email network, except for a few changes. First, the experimental results for each class of the synthetic networks are averaged over 30 randomly generated network topologies. Another difference lies in how the targeted set  $\mathcal{S}$  is selected. For each randomly generated network, the targeted set  $\mathcal{S}$  is selected as the node whose degree is the 90 percentile of the degree sequence, and its neighbors. Some statistics of the synthetic networks are summarized in Table 1. Recall that  $\delta = 0.24$  and  $\beta = 0.06$ . The experimental results are showed in Figure 4. The conclusion derived from Figure 4 is similar to that of the email network. It is worth pointing out that maximizing the normalized cut of  $\mathcal{S}$  is effective on BA networks, while for other network it may backfire.

	BA	Small-World	BTER
$ \mathcal{S} $	17.5	12	20.03
$d_{min}$	9.86	10	11.69
density	0.02	0.03	0.03
average degree	9.87	10	11.5
average clustering coeff.	0.08	0.35	0.05

Table 1: Statistics of synthetic networks.

## 5 Additional Results for Different Values of $\delta$ and $\beta$

In the main paper,  $\delta = 0.24$  and  $\beta = 0.2$  for the airport and brain networks, while  $\delta = 0.24$  and  $\beta = 0.06$  for the email network. The ratio  $\delta/\beta$  is 1.2 for the former two networks, while 4 for the latter. In what follows we explore the effectiveness of our model in different regimes of  $\delta/\beta$ . For the airport and brain networks, we present results for  $(\delta = 0.5, \beta = 0.1)$  and  $(\delta = 0.3, \beta = 0.5)$ . The former (resp. latter) corresponds to the regime above (resp. below) 1.2. The results for the airport network are showed in Figure 5, and the results for the brain network are in Figure 6. For the email network we present results for  $(\delta = 0.5, \beta = 0.1)$  and  $(\delta = 0.3, \beta = 0.5)$ , also corresponds to the regime above and below the original ratio respectively. The results are showed in Figure 7. The conclusions are consistent with that presented in the main paper.

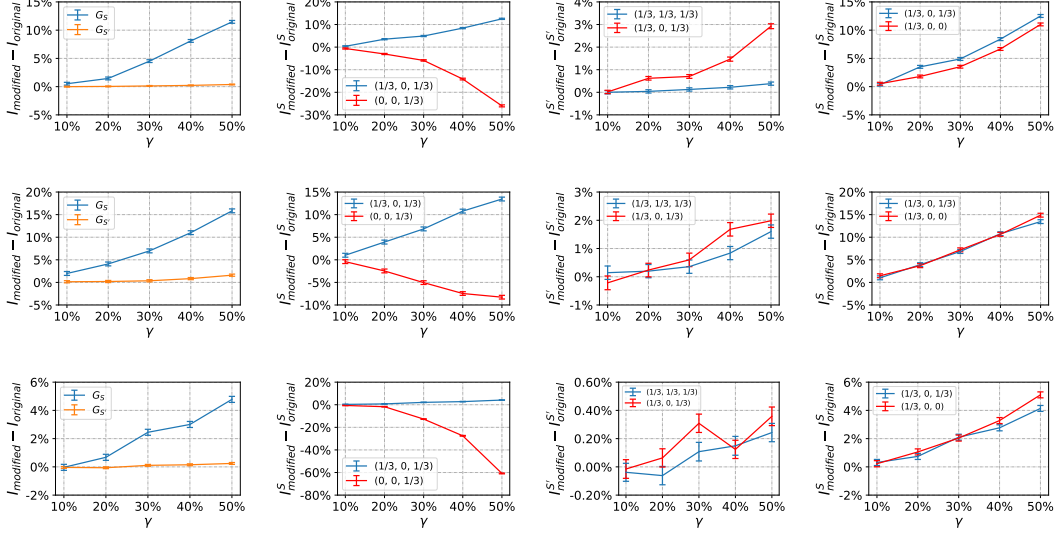


Figure 4: Experimental results on synthetic networks. The first column shows the overall effectiveness of the threat model. Remaining columns show the effectiveness of: 1) maximizing  $\lambda_1(\tilde{\mathbf{A}}_S)$ ; 2) Maximizing the eigenvector centrality of  $\mathcal{S}$ ; 3) maximizing the normalized cut of  $\mathcal{S}$ . **Top:** BA; **Middle:** Small-World; **Bottom:** BTER

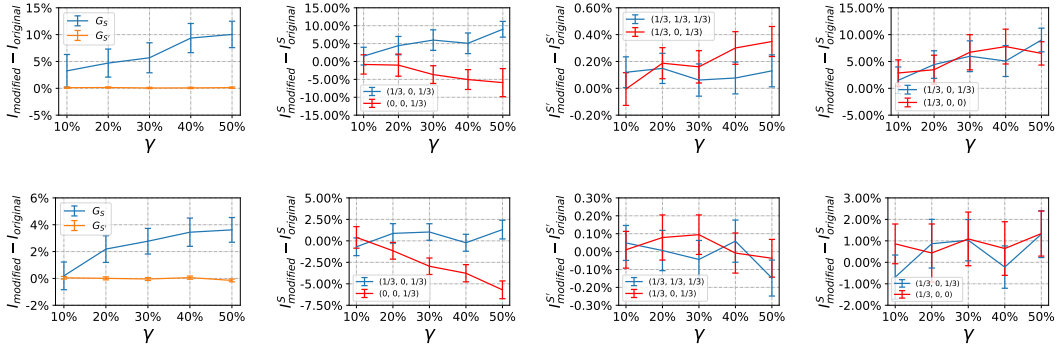


Figure 5: Experimental results for different  $\delta$  and  $\beta$  values on the airport network. **Top:**  $\delta = 0.5, \beta = 0.1$ ; **Bottom:**  $\delta = 0.3, \beta = 0.5$ .

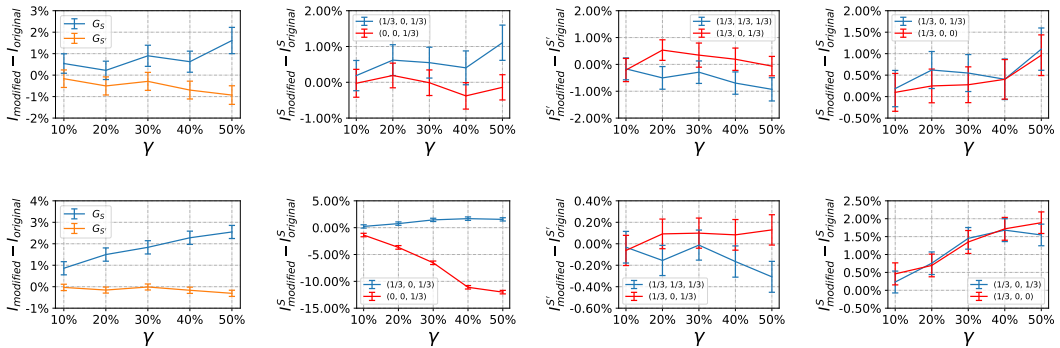


Figure 6: Experimental results for different  $\delta$  and  $\beta$  values on the brain network. **Top:**  $\delta = 0.5, \beta = 0.1$ ; **Bottom:**  $\delta = 0.3, \beta = 0.5$ .

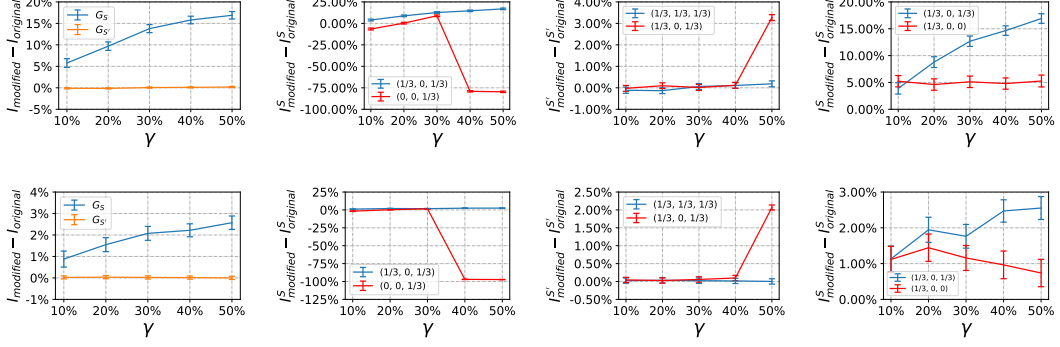


Figure 7: Experimental results for different  $\delta$  and  $\beta$  values on the email network. **Top:**  $\delta = 0.5, \beta = 0.1$ ; **Bottom:**  $\delta = 0.3, \beta = 0.5$ .

## 6 Experimental Results for the Certified Robustness

We run several experiments on synthetic networks to verify the certified robustness. The experimental setup is basically the same as that in Appendix 4, except that we explore a wider range of values for budget  $\epsilon$ . The minimum degree  $d_{min}$  for each class of network is listed in Table 1. Recall that the parameters of diffusion are  $\delta = 0.24$  and  $\beta = 0.06$ ; the condition  $\delta/\beta \leq d_{min}$  is satisfied. The results are showed in Fig. 8. The blue lines represent the difference  $I(\tilde{G}_S) - I(G_S)$ . As we mentioned before, the objective of targeted diffusion is to maximize the difference. Note that here  $I(\tilde{G}_S)$  and  $I(G_S)$  are estimated from actual simulations. The x-axis is the budget  $\epsilon$ , which ranges from  $0.01\lambda_1(\mathbf{A})$  to  $0.5\lambda_1(\mathbf{A})$ . The red vertical lines are the lower bounds of  $\epsilon$  computed from Eq. (12) in Theorem 1. Observe that when  $\epsilon$  is less than the lower bound (the left of the red line), the difference  $I(\tilde{G}_S) - I(G_S)$  is close to zero, which indicates that the network is robust against targeted diffusion, i.e., the principal cannot significantly increase  $I(G_S)$  through graph modification.

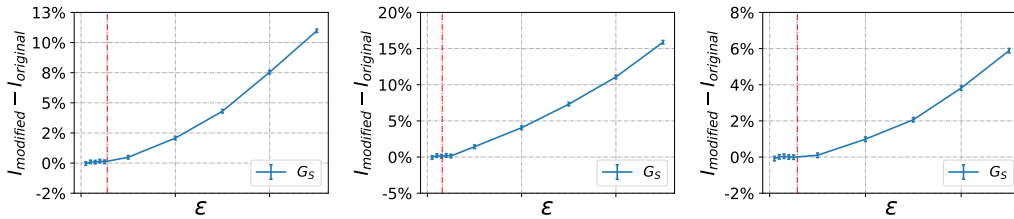


Figure 8: Experimental results for the certified robustness. **Left:** BA, **Middle:** Small-World, **Right:** BTER.